Trinity College Dublin
Coláiste na Tríonóide, Baile Átha Cliath
The University of Dublin

Using MRI to evaluate neurodevelopment in a mouse model of neonatal hypoxia

This thesis submitted to the University of Dublin, Trinity College for the degree of Master of Science in Physiology

Ronan Murphy

26/11/2025

Supervisor:
Eva Jimenez-Mateos,
Discipline of Physiology,
School of Medicine,
Trinity College Dublin

Co-Supervisors:
Jason Wyse and Arthur White,
School of Computer Science and Statistics,
Trinity College Dublin

Plagiarism Declaration

I declare that this thesis has not been submitted as an exercise for a degree at this or any other university and it is entirely my own work.

I agree to deposit this thesis in the University's open access institutional repository or allow the Library to do so on my behalf, subject to Irish Copyright Legislation and Trinity College Library conditions of use and acknowledgement.

I consent to the examiner retaining a copy of the thesis beyond the examining period, should they so wish (EU GDPR May 2018).

Signed

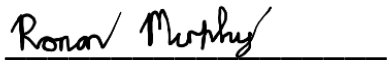

Date

26/11/2025

Summary

Neonatal hypoxia is a medical condition resulting from the deprivation of oxygen to a newborn infant lasting long enough to cause harm to the brain. It remains a serious condition that causes significant mortality (1 million neonatal deaths per year worldwide) and morbidity, including cerebral palsy, epilepsy, and learning disabilities. Current diagnostics and treatment have limitations; there is an unmet medical need to understand the pathophysiology of neonatal hypoxia to find novel diagnostic tools that can support effective therapies. This study aimed to characterise anatomical brain changes associated with a postnatal day 7 mouse model of neonatal hypoxia and to investigate their impact on neurological development and behaviour. It was observed that hypoxia-exposed pups exhibited delayed reflex development and impaired locomotion. Adolescent mice previously exposed to hypoxia demonstrated cognitive and behavioural impairments, highlighting the long-term effects of early oxygen deprivation. MRI analysis revealed hippocampal oedema, which correlated with impairments across multiple behavioural assessments. These findings provide critical insight into the pathological progression of hypoxic injury and open new avenues to diagnostic tools.

Acknowledgments

First and foremost, I would like to express the utmost gratitude to my supervisor, Dr. Eva Jimenez-Mateos, for her continued support and advice throughout the course of my master's degree. From day one, she has been a constant source of encouragement and guidance in the carrying out of this research, facilitating my learning, and assisting when needed. Without her immense effort, this thesis would not have been possible.

Secondly, I would like to thank Ms. Jessie Kingston, who was responsible for the collection of data from animal behavioural experiments carried out for the purpose of this project. I am incredibly grateful for the time and effort she has put in during this project, providing training and collaboration, and assisting in every aspect of this thesis, from data generation to technical support.

I also wish to acknowledge the contributions of my co-supervisors, Dr. Jason Wyse and Dr. Arthur White, from the School of Computer Science and Statistics, for their help with programming and statistical queries, as well as Dr. Jeffrey Glennon, from the Biomedical Facility in UCD, for facilitating my use of their rodent MRI scanner.

Finally, an enormous thanks is due to all members of the Jimenez lab, past and present, who have contributed to such a pleasant working environment over the past two years. In particular, I would like to mention Dr. Aisling Leavy, Mr. Harry Frost, and Ms. Ashla Copeland.

Contents

List of Figures and Tables

List of Abbreviations

Abbreviation	*Definition*
ATP	Adenosine Triphosphate
CSF	Cerebrospinal Fluid
DWI	Diffusion Weighted Imaging
FLASH	Fast Low Angle Shot
GM	Geometric Mean
HIE	Hypoxic-Ischemic Encephalopathy
MEMRI	Manganese-Enhanced Magnetic Resonance Imaging
MW	Mann-Whitney
NE	Neonatal Encephalopathy
OCD	Obsessive Compulsive Disorder
OS	Oxidative Stress
P	Postnatal Day
PBS	Phosphate-Buffered Saline
PCA	Principal Component Analysis
PFA	Paraformaldehyde
RARE	Rapid Acquisition with Refocusing Echoes
SEM	Standard Error of the Mean
TH	Therapeutic Hypothermia

Introduction

Hypoxic-ischemic encephalopathy

Neonatal encephalopathy (NE) is a broad term describing brain dysfunction caused by a lack of cerebral blood flow to the brain, mainly caused by hypoxic-ischemic encephalopathy (HIE). NE is a form of this condition that develops within the first few days of life and is characterised by impaired neurological function, reduced muscle tone, and difficulty maintaining respiration. (Aslam et al., 2019).

Neonatal hypoxia is caused by deprivation of oxygen to an infant's brain during birth and poses significant risks in terms of complications at birth and long-term neurodevelopmental impairments. Labour and delivery complications, such as placental abruption, prolapse of the umbilical cord, uterine rupture, or shoulder dystocia, can contribute to this oxygen deprivation. These conditions obstruct oxygen delivery to the brain by blocking placental perfusion or by impairing blood flow through the umbilical cord (Douglas-Escobar & Weiss, 2015).

HIE is one of the leading causes of neonatal mortality, accounting for over 25% of infant deaths (Volpe, 2001). Mortality rates range from 10 to 60%, with many survivors experiencing significant neurodevelopmental disabilities (Shah M. S., 2025). The prevalence of HIE varies globally and occurs in 1–8 births per 1000 in developed countries, and this figure can increase up to 26 births per 1000 in developing countries (Douglas-Escobar & Weiss, 2015). These disparities highlight the need for novel treatments to reduce HIE incidence through improved postnatal care and better prognostic tools for neurological outcomes.

Pathophysiology of neonatal hypoxia

A hypoxic injury is an evolving injury that can last days or weeks, and often leads to long-term neurodevelopmental effects (Douglas-Escobar & Weiss, 2015). Due to a lack of oxygen in a hypoxic event, there is a metabolic switch to anaerobic glycolysis, which results in a depletion of adenosine triphosphate (ATP) production and leads to a cascade of cell-damaging events. There are multiple phases of a hypoxic injury (Figure 1). The primary phase occurs within the first hour after injury and is involved in the recovery of oxidative metabolism (Yıldız et al., 2017). This is succeeded by the latent phase between hours 1-6, in which hypoperfusion, oxidative stress, and inflammation occur. The secondary phase takes place between 6 and 72

hours and involves the accumulation of cytotoxic oedema, excitotoxicity, secondary energy failure, and the onset of seizures. These processes severely damage the cells and lead to an activation of apoptotic pathways and an increase in inflammation (Greco et al., 2020). The tertiary phase occurs weeks to months later and is characterised by late cell death, brain remodelling, and astrogliosis (Douglas-Escobar & Weiss, 2015).

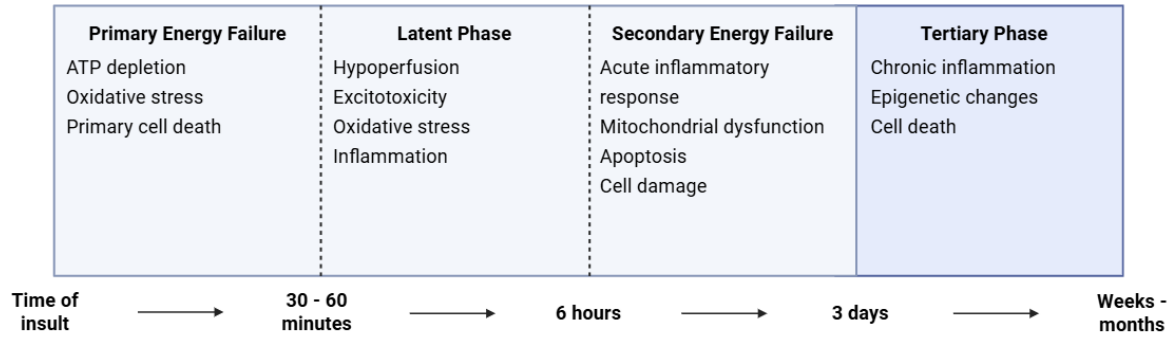

Figure 1: Pathophysiology of neonatal hypoxia. Created with BioRender.com and adapted from Douglas-Escobar & Weiss *(Douglas-Escobar & Weiss, 2015)*.

Treatment of neonatal hypoxia

Following neonatal hypoxia, a limited number of therapeutic options are available to clinicians. The gold standard for treatment is therapeutic hypothermia (TH), in which the body temperature of the newborn is lowered to 33.5°C for 72 hours to slow down metabolism and reduce inflammation (Tetorou et al., 2021). However, TH has limitations to its neuroprotective effects, with 40% of patients still developing negative neurological outcomes. It also needs to be applied within six hours of the hypoxic event, known as the therapeutic window, for successful recovery. Understanding how hypoxia affects postnatal brain development is critical for improving treatment strategies and long-term outcomes.

Magnetic resonance imaging

MRI is an essential tool for diagnosing neonatal hypoxia. It plays a crucial role in research by providing insights into the progression of pathophysiological changes and dynamic processes involved in hypoxic development in brain structure and function (Ehlting et al., 2022). MRI has several advantages over histology due to its ability to generate 3D, digital, whole-brain longitudinal data (Wu & Zhang, 2016). MRI has many different sequences available to use for varying purposes. T1-weighted imaging is preferred in examining anatomical structures, while T2-weighted scans are used to detect brain pathology (Zhou et al., 2017).

Manganese has been used as a contrast agent to enhance the MRI visualisation in T1-weighted scans (Qiu et al., 2018). T2-weighted imaging is particularly important in neonatal brains, as there is a higher water content compared to the adult brain due to ongoing myelination (Ferriero, 2004). This dual-modal MRI approach allows for more accurate spatial and temporal imaging and is valuable in aiding the identification of neuroanatomical and pathological changes in the hypoxia-exposed brain.

Hippocampal damage

Early-life insult to the brain may impede normal maturation, rendering it susceptible to neurodevelopmental disorders (Adams-Chapman, 2009). Severe hypoxia typically manifests in an MRI as abnormally high-intensity signals in key brain areas such as the hippocampus, basal ganglia, thalami, corticospinal tract, white matter, putamen, vermis, and cortex (Douglas-Escobar & Weiss, 2015). The hippocampus is particularly vulnerable to atrophy following a hypoxic event, largely due to the loss of highly sensitive CA1 and CA3 neurons, which has been seen to result in reduced hippocampal volume (Aggarwal et al., 2014).

Hypoxic injury in the brain leads to both early and delayed neuronal damage, with the mechanism of cell damage varying based on timing, brain region, and neuronal connectivity (Ristovska et al., 2022). The cellular damage that occurs after a hypoxic injury leads to brain oedema and swelling due to the activation of microglia and astrocytes, the glial cells of the brain, which has ultimately been seen to correlate with neurological disorders (Machie et al., 2021).

Neurological outcomes

Hippocampal structural changes have been linked to neurodevelopmental deficits later in life (Brait et al., 2021). The number of babies that develop neurodevelopmental conditions due to HIE is approximately 400,000 per year (Chen et al., 2023). The severity of the long-term outcome is directly linked to the severity of the hypoxic event. Neonates exposed to both prolonged partial hypoxia and acute near-total hypoxia developed the most severe neurodevelopmental outcomes compared to each group independently (Shah & Perlman, 2009). Some of the acute symptoms are seizures, reduced consciousness, weak breathing, and poor muscle tone (Greco et al., 2020). Neurological outcomes that develop after HIE include cerebral palsy (~10-20%), visual & auditory problems (~40%), motor impairments, behavioural

impairments, intellectual disability, and social disorders (Yıldız et al., 2017). Other studies show that 5-10% of infants will develop deficiencies in motor skills, and 20-50% will demonstrate sensory or cognitive impairments (Volpe, 2001).

Neurological outcomes in mice

Work has already been done to show that MRI scans can correlate structural changes to functional behaviours in mice (Adén et al., 2002). MR imaging showed that lesions reached maximum size at 3-6 hours post-hypoxia, and this damage correlated to decreased forward locomotion and unilateral hypotrophy. Other studies have shown that cognitive, memory, and behavioural impairments, along with aggression and hyperactivity, can be seen in rodents with hippocampal damage (Brait et al., 2021). Behavioural tests such as negative geotaxis, beam walking tests, and the Morris water maze test have shown impairments in sensorimotor functions, exploratory behaviour, and spatial learning, and correlated this to a reduction in brain volume induced by hypoxic injury (Zanier et al., 2013).

Current need for further research

There is a need for further study to characterise the anatomical brain changes that occur in hypoxia-exposed brains and to further understand the neurological impacts these changes have on the behaviour and neurological development of neonatal hypoxia mouse models. There has been some work to characterise these effects in HIE models that include an ischemic element, producing a localised injury in the brain (Brait et al., 2021). However, no work has been completed to characterise these effects in a global hypoxic model of neonatal hypoxia.

The aims of this project are: (1) to examine the effects of hypoxia on neonatal and adult reflexes and behaviours, (2) to characterise structural brain changes that occur in the brain post-hypoxic injury, and (3) to investigate a possible correlation between brain damage and behavioural impairment, which may support prognostic tools and novel therapies. The hypothesis will be tested as to whether the MRI analysis of structural brain changes coincides with adverse neurological damage displayed in behavioural tests in a mouse model of neonatal hypoxia.

Methods

Animals

All animal experiments adhered to the guidelines set by the European Communities Council Directive (86/609/EEC, 2010/63/EU) and were conducted under a license issued by the Department of Health and the Health Products Regulatory Authority, Ireland (AE19136/P140). Ethical approval was granted by the Trinity College Dublin Animal Research Ethics Committee. Neonatal C57BL/6J mouse litters (mean weight 3.43 ± 0.41g; aged postnatal day 6.5–7.5 (P7)) were sourced from the Comparative Medicine Unit in Trinity College Dublin. Pups remained with their dams in a barrier-controlled environment, maintained on a 12-hour light-dark cycle with unrestricted access to food and water. Animals were assessed daily to monitor overall health status. Experimental numbers were calculated using the two-tailed t-test power analysis function (significance level = 0.05, power = 0.8, effect size = 1.6) in G*Power version 3.1.9 (Kang, 2021). All experimental procedures took place in the morning during the light phase.

Hypoxia model

All live animal procedures were carried out by Ms. Kingston. Male and female pups from the same litter were randomly assigned to one of two groups: hypoxia or control. The hypoxia induction procedure was performed as previously established (Rodriguez-Alvarez et al., 2015). At postnatal day 7 (P7), pups were placed in a hypoxia chamber and exposed to a mixture of 5% O_2 and 95% N_2 for 15 minutes to induce hypoxia (Figure 2). An O_2 monitor continuously measured oxygen levels within the chamber throughout the procedure. To prevent the possibility of hypothermia, the temperature was maintained at 34°C using an incubator. Humidity was kept constant at 80%. Control pups underwent a sham procedure in the chamber, exposed to room air (21% O_2) for the same duration. Following the procedure, all pups were returned to their dams.

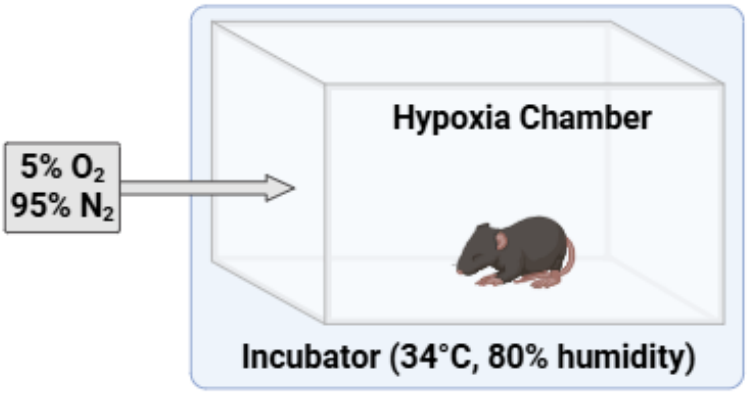

Figure 2: Illustration of hypoxia induction. Apparatus used to induce hypoxia in P7 pups. Created with BioRender.com

Neonatal behaviour

A battery of motor tests was performed at postnatal days 8 and 10 (P8 and P10), at 24- and 72-hours post-hypoxia (Figure 3). This consisted of ambulation, hindlimb foot angle, negative geotaxis, surface righting, grip strength, and cliff aversion tests (Feather-Schussler & Ferguson, 2016). Tests were not repeated to avoid learning. Pups were separated from their dams for the shortest time possible (mean time 23.5 ± 3 minutes) to minimize stress from maternal separation. All pups underwent routine welfare checks before testing to confirm normal development.

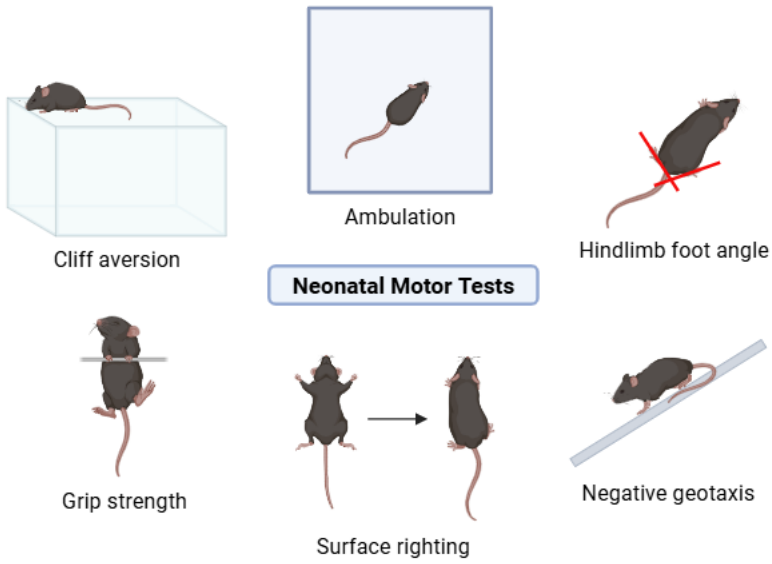

Figure 3: Illustration of neonatal tests. Neonatal motor tests performed at P8 and P10. Created with BioRender.com

Ambulation

Pups were placed in a flat arena and allowed to move freely for 3 minutes. If a pup remained stationary, gentle prodding on the back was used to encourage movement. Video recordings were analysed to assign each pup an ambulation score based on a 7-point system adapted from Feather-Schussler and Ferguson (Table 1: Scoring system for ambulation test. Symmetrical limb movement was characterised by the coordinated alignment of the hind paws with the front paws as the mouse walked. In contrast, asymmetric limb movement was identified by irregular positioning of the limbs and disrupted coordination. Crawling and walking were distinguished based on the areas of the hindlimb that were in contact with the ground. During crawling, the entire hind paw, including the heel, maintained contact with the surface, whereas in walking, only the toes touched the ground (Feather-Schussler & Ferguson, 2016).

Movement	Score
No movement	0
Lots of turning, encouragement needed, little/no straight crawling	0.5
Crawling with asymmetric limb movement	1
Crawling with sporadic, symmetric limb movement	1.5
Slow crawling with symmetric limb movement	2
Fast crawling with symmetric limb movement	2.5
Walking with symmetric limb movement	3

Table 1: Scoring system for ambulation test

Hindlimb foot angle

The ambulation test videos were also used to measure the hindlimb foot angle of each pup. Three images of each pup were captured after the pup had completed a full step with both back paws flat on the ground (Feather-Schussler & Ferguson, 2016). The angle between the lines connecting the middle digit to mid-heel was measured using FIJI software (Schindelin et al., 2012), as shown in Figure 4, and the mean hindlimb foot angle for the three images was calculated. Analysis was performed by two independent researchers, and the mean of their results was recorded.

Figure 4: Hindlimb foot angle measurement using FIJI

Surface righting

Each pup was positioned on its back and secured by holding both the front and hind paws for five seconds before being released. The time required for the pup to transition from lying on its back to righting itself onto its paws was recorded. (Feather-Schussler & Ferguson, 2016).

Negative geotaxis

Each pup was positioned on a downward slope with its head facing down. The pup was gently held in place for five seconds before the test began. The time taken to turn around and face upward was recorded. Pups were given a maximum of 30 seconds to complete this test. Any mouse that did not turn to face upward after 30 seconds was recorded as a non-participant (Feather-Schussler & Ferguson, 2016). A scoring system was devised to classify the mice into categories of responsiveness to the test, in order to include non-participants in analysis. The data was standardised to the geometric mean (GM) of all participating controls, as outlined in Table 2: Scoring system for negative geotaxis test.

Time for the mouse to turn upwards	Score
Did not participate	0
Slower than 150% of GM	1
Quicker than or equal to 150% of GM	2

Table 2: Scoring system for negative geotaxis test

Grip strength

Grip strength was evaluated by allowing each pup to grasp a cotton swab with both front limbs while keeping its hind limbs on the ground. Once a firm grip was established, the swab was lifted, suspending the pup in the air. The time taken to release the grip was recorded. Those

that did not attempt to hold on or those that attempted to support themselves by swinging their legs onto the swab were excluded from the analysis (Feather-Schussler & Ferguson, 2016).

Cliff aversion

A cliff-like surface was set up, raised from ground level in an enclosed space. Before each test, the cliff-like surface was pre-scented with the mother for 3 minutes. Each pup was positioned at the edge of the elevated surface, with its front paws and snout overhanging the edge. The time taken to withdraw both the snout and front paws from the edge was recorded. If the pup did not turn within 30 seconds, it was recorded as a non-participant (Feather-Schussler & Ferguson, 2016).

The results of this test were standardised by litter due to the olfactory guiding required to perform the test, with different mothers emitting different levels of pheromones. A scoring system was created to classify the mice into categories of responsiveness to the test, in order to include non-participants in analysis. This was done as previously described in the negative geotaxis test. In each litter, the data were standardised to the geometric mean (GM) of all participating controls in the litter, as outlined in Table 3: Scoring system for cliff aversion test If 50% or more of the controls in a litter did not participate in the test, then the entire litter was excluded from scoring due to lack of a reliable control average time.

Time for the mouse to turn around	Score
Did not participate	0
Slower than 150% of GM	1
Quicker than or equal to 150% of GM	2

Table 3: Scoring system for cliff aversion test

Adolescent behaviour

Behavioural testing was carried out on adolescent mice from 3 to 5 weeks post-hypoxia (P28–40). This consisted of marble burying, light-dark box, open field, and novel object location tests. 72 hours were provided between tests to allow the mice to recover. These tests were recorded and analysed using ANY-maze video tracking software version 7.4 (Stoelting Europe).

Marble burying

The marble burying test was performed on 4-week-old (P28) mice to evaluate repetitive and compulsive-like behaviours (de Brouwer et al., 2019). The test was carried out in a mouse cage

covered with a transparent plastic sheet and filled with sawdust bedding to a depth of 5cm. 12 glass toy marbles of different colours were arranged in a 3 x 4 grid on the surface of the bedding (Figure 5). Each mouse was placed inside the cage and left undisturbed in the room for 30 minutes. After each trial, the marbles were washed and put back in fresh bedding. Video recordings of each trial were collected and the number of marbles buried entirely below the sawdust at the end of the video were counted.

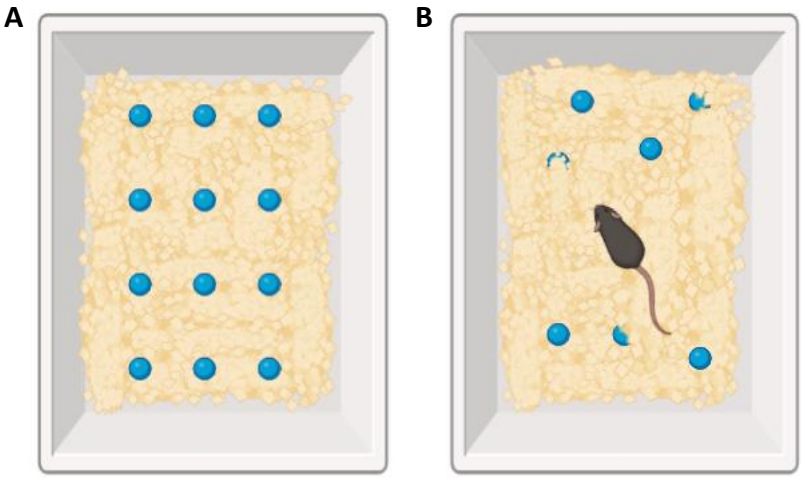

Figure 5: Illustration of marble burying test. Positioning of marbles **(A)** before and **(B)** after the test. Created with BioRender.com

Light-dark box

Anxiety-like behaviour was evaluated using the light-dark box test, following the protocols previously described (Forcelli et al., 2012). The test apparatus consisted of a lit chamber connected to a dark chamber through a small opening (Figure 6). The light area was illuminated from above by a white lamp bulb, accompanied by background white noise. Each mouse was placed in the light chamber, facing away from the entrance to the dark chamber, and was allowed to explore the apparatus for 10 minutes.

The tests were recorded using ANY-maze video tracking software, and video footage was analysed. The latency to enter the dark chamber for the first time was manually recorded using a stopwatch, stopping once the entire body of the mouse, excluding the tail, had passed through the opening. Timing measurements were conducted by two independent researchers, and the mean of their recorded times was calculated.

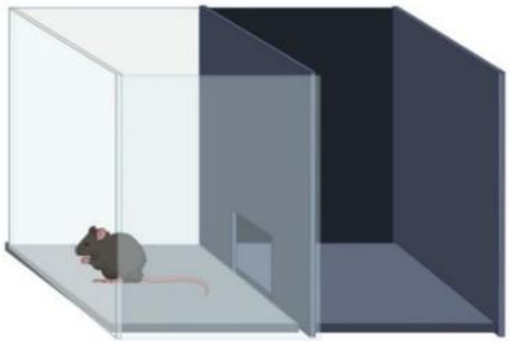

Figure 6: Illustration of light-dark box test. Created with BioRender.com

Open field

The open field test is used to assess locomotor activity and is performed before conducting the novel object location test. The mice were placed in an open-field arena (Figure 7) and allowed to explore the space freely for 10 minutes (Oliveira et al., 2010). Their movement was tracked using ANY-maze video monitoring software, in which key metrics such as total distance travelled, time spent in motion, and average speed were recorded. Data visualization tools, including track plots and heat maps, were generated in ANY-maze to analyse their activity patterns.

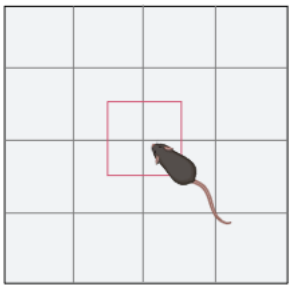

Figure 7: Illustration of open field test. Created with BioRender.com

Novel object location

The novel object location test assesses the hippocampal spatial memory function of mice. This test was based on the protocol previously described (Oliveira et al., 2010). This test was carried out over 2 consecutive days in 10-minute sessions. The first day was habituation day. The mice explored an area without objects for 10 minutes (this session was used as the open field test). This was followed by three 10-minute sessions with two objects (Figure 8.A). The second day was the test day, and one of the objects was moved to a novel position in the box (Figure 8.B). The objects were removed and cleaned between each trial. The mice were

recorded for 10 minutes as they explored the box, and this video was analysed through manual observation using a hand-held stopwatch. The number of times the mouse visited each object and the time it spent exploring each object was recorded. A visit consisted of the mouse interacting with the objects with their nose or paw within 1cm.

Results of this test were adjusted to account for any preference each mouse had shown towards one object over another in the familiarisation stage. The correction factor was defined as the time spent interacting with object 2 (the object to later be moved) as a percentage of total time spent interacting with either object in the three familiarisation phases, divided by 50. In this way, a score of below 1 indicated a preference for object 1, while a score of above 1 indicated a preference for object 2. A score of exactly 1 indicated no preference towards either object.

In the novel object location stage, the time spent interacting with object 2 (now in the novel location) was measured as a percentage of total time spent interacting with either object in this phase. This figure was divided by the previous correction factor to obtain the adjusted percentage. This analysis was performed by two independent researchers, and the mean of their results was calculated.

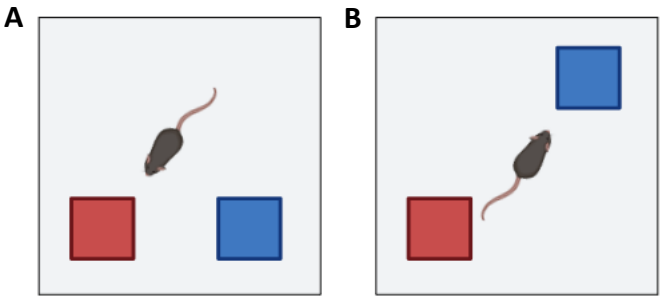

Figure 8: Illustration of novel object location test Apparatus setup for **(A)** familiarisation stage and **(B)** novel object location stage. Created with BioRender.com

MRI

MRI preparation

The mice were prepared for scanning using MEMRI (manganese-enhanced magnetic resonance imaging). 24 hours before the scan, mice received a 0.4 mmol/kg dose of 30 mM manganese chloride (MnCl2) solution. For P42 mice, the manganese was administered by intraperitoneal injection. For P10 pups, the manganese was administered to the mother by intraperitoneal injection 24 hours before scanning and delivered into the neonates through

maternal milk. Both P10 and P42 mice were euthanised by transcardiac perfusion with phosphate-buffered saline (PBS) followed by 4% paraformaldehyde (PFA) as previously described (Wu et al., 2021). PBS/PFA fixation of the tissue was carried out to clear blood from the brain and to preserve it while the MRI scans took place.

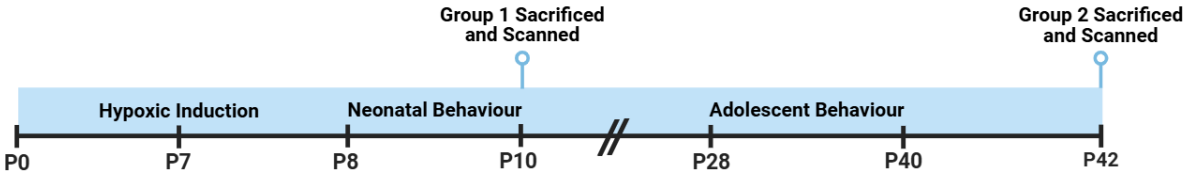

Figure 9: Timeline of experimental events. Created with BioRender.com

MRI scans

MRI scans were carried out on the same day the mice were euthanised, to ensure that the manganese was still viable in the brain (Sato et al., 2018). The mice were scanned using a BioSpec 94/20 Bruker 9.4 Tesla MRI machine (Figure 10.B). The mice were placed into the thumb of a white nitrile glove and placed into the mouse bed of the MRI machine. The specimen was secured in place via a tooth bar to the front of the head and ear bars to the side of the head (Figure 10.A). The head coil (^{1}H receive-only 2 x 2 mouse brain surface array coil, Bruker) was placed over the head, and the scans were carried out.

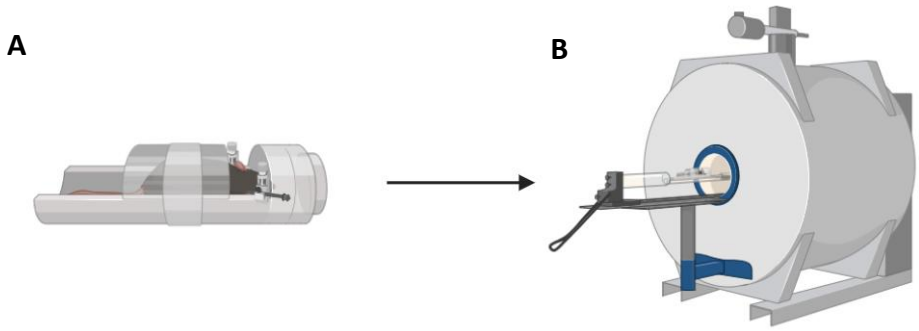

Figure 10: Illustration of MRI apparatus. **(A)** Positioning of the specimen in the mouse bed. **(B)** Rodent MRI scanner. Created with BioRender.com

A single-slice localiser scan was carried out first, followed by a multi-slice localiser, in order to position the field of view for the subsequent scans. T1-weighted FLASH 3D isotropic (Qiu et al., 2018) and T2-weighted TurboRARE 2D (Doman et al., 2018) scans were taken to assess the anatomical structures and pathological damage, respectively, within the brain. T1- and T2-weighted scans were contiguous (i.e., no slice gaps) for the purpose of volumetric analysis. Total imaging time per mouse was approximately 30 minutes.

Sequence	Repetition Time (ms)	Echo Time (ms)	Number of Excitations	Matrix	Field of View (mm)	Number of Slices	Slice Thickness (mm)	Slice Gap (mm)	Resolution (mm)	Acquisition Time (mm:ss)
Localiser	100	2.3	1	256 * 256	40 * 40	1	1	N/A	0.15625 * 0.15625	0:13
Localiser Multislice	15	3	3	192 * 192	25 * 25	5	1	1	0.13021 * 0.13021	2:10
T1 FLASH 3D Isotropic	26	6.5	2	192 * 192 * 60	19.2 * 19.2 * 6	60	0.1	0	0.1 * 0.1 * 0.1	11:09
T2 TurboRARE 2D	5500	57.75	4	256 * 256	19.2 * 19.2	20	0.3	0	0.075 * 0.075	11:44

Table 4: MRI settings for each sequence used.

MRI analysis

MRI analysis was conducted using ITK-SNAP software (Yushkevich et al., 2006). ITK-SNAP is a semiautomated segmentation software that is used to aid in manual segmentation of image analysis. MRI scans of the mouse brains can be viewed in the coronal, axial, and sagittal planes in three out of the four windows. The fourth window contains a 3D structure of the segmented images (Figure 11).

Manual slice-by-slice segmentation was completed in the coronal plane. The right and left hippocampi were traced by the researcher in both T1- and T2-weighted scans and labelled using a manual segmentation technique. Contrast was adjusted manually to correctly view the hippocampal boundary. This was confirmed through comparison with the Allen Mouse Brain Atlas (atlas.brain-map.org). Measurements were also taken of any cytotoxic oedema (hyperintense regions) in the hippocampus in T2-weighted scans. The minimum threshold for hyperintensity was defined as the intensity present in the third ventricle. Cerebrospinal fluid (CSF) and oedema appear at a similar level of intensity, so oedema was distinguished from CSF as hyperintensity in areas where it was not expected. Accuracy could be enhanced by decreasing the overall label opacity to allow for a clearer visualisation of the hippocampal boundaries. Volumetric analysis was calculated based on the number of voxels in each segment.

The analysis of each brain took approximately one hour. All segmentations were carried out by two independent researchers and subsequently compared. If the volumes agreed within a 10% margin, the mean value of the two results was taken. If this did not occur, a mutual segmentation was performed by both researchers together. There was disagreement for 3 of the 16 T1-weighted scans and 8 of the 23 T2-weighted scans.

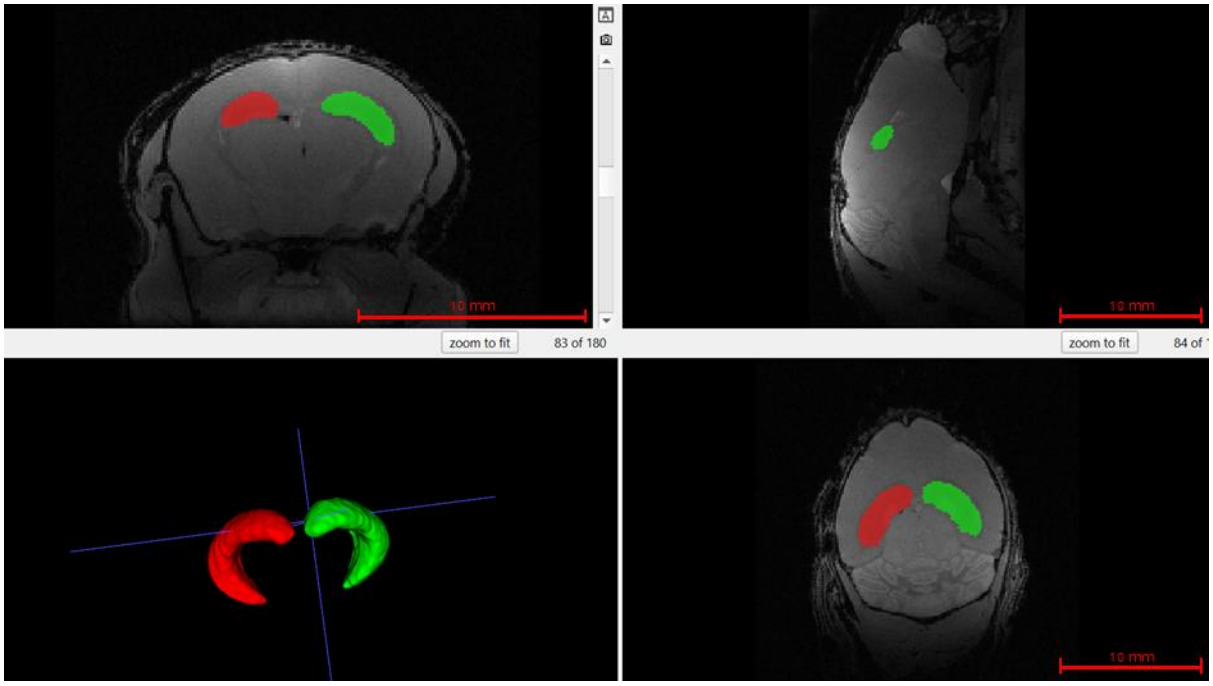

Figure 11: ITK-SNAP hippocampal segmentation. The top-left, top-right, and bottom-right windows represent the coronal, sagittal, and axial planes, respectively. The bottom-left window displays the 3D reconstruction of the segmented hippocampus, with the right hippocampus in red and the left hippocampus in green. Note: the scans are shown according to radiological convention, with the left side of the brain displayed on the right side of the image.

Statistical methods

All continuous data were presented as mean ± standard error of the mean (SEM) and all discrete data were presented as violin plots. All statistical tests were carried out using GraphPad Prism version 10.4.1. All comparisons between groups were performed using Mann-Whitney (MW) non-parametric tests, and all correlations were performed using Pearson's correlation coefficient. Statistical significance was defined as $p < 0.05$ for all comparisons. Principal component analysis (PCA) was generated using R version 4.4.0. Data were first scaled and centred around 0, then PCA was performed using the prcomp function. A scatter plot of the data with the first two principal components as the axes was generated using the ggplot2 package (Wickham, 2016).

Results

Neonatal behaviour

Significantly lower ambulation scores displayed in hypoxia-exposed pups than in controls 72h post-hypoxia

A total number of 33 mice underwent this test, 16 control (8 male, 8 female) and 17 hypoxia (8 male, 9 female). 2 controls were excluded from the analysis at both 24h and 72h post-hypoxia as the videos were missing. There is no statistical significance between the groups 24h post-hypoxia; however, by 72h, ambulation scores are significantly lower (p=0.0004) in hypoxia-exposed pups than in the healthy controls (Figure 12).

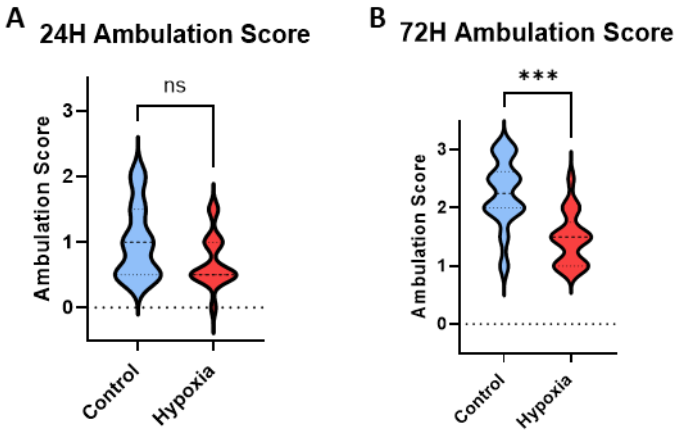

Figure 12: Ambulation test results. **(A)** 24h post-hypoxia (MW test, control n=14, hypoxia n=17, p=0.1391). **(B)** 72h post-hypoxia (MW test, control n=14, hypoxia n=17, p=0.0004).

Significantly larger hindlimb foot angles exhibited by hypoxia-exposed pups than controls 72h post-hypoxia

A total number of 33 mice underwent this test, 16 control and 17 hypoxia. As this test uses the ambulation videos, it is also missing 2 controls at both 24h and 72h post-hypoxia. There was a near-significant difference (p = 0.0568) in hindlimb foot angle between the groups at 24h post-hypoxia, and by 72h, hypoxia-exposed mice demonstrated significantly larger (p=0.0002) hindlimb foot angles than healthy controls (Figure 13).

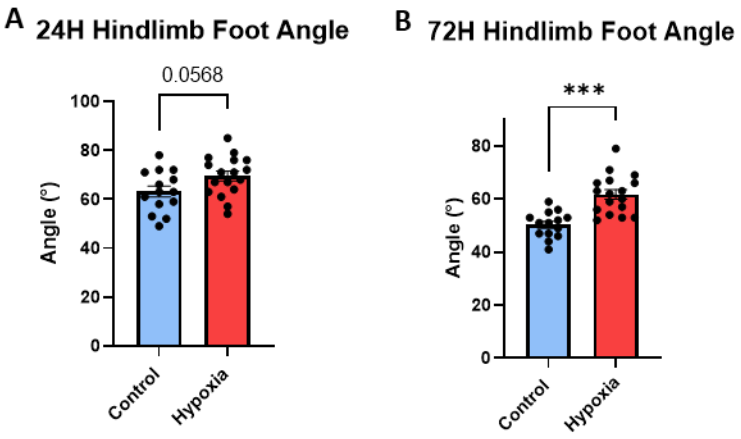

Figure 13: Hindlimb foot angle test results. **(A)** 24h post-hypoxia (MW test, control n=14, hypoxia n=17, p=0.0568). **(B)** 72h post-hypoxia (MW test, control n=14, hypoxia n=17, p=0.0002).

No significant difference observed between hypoxia-exposed pups and controls in other neurological tests

A total number of 33 mice underwent the surface righting test, 16 control and 17 hypoxia. There was no significant difference in surface righting times between the control and hypoxia groups at either 24h or 72h post-hypoxia (Figure 14).

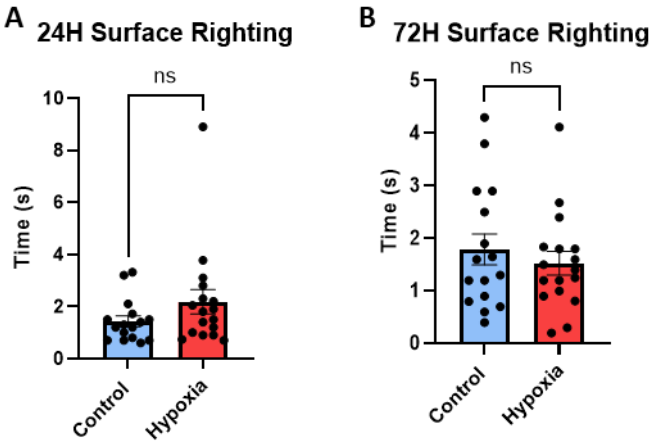

Figure 14: Surface righting test results. **(A)** 24h post-hypoxia (MW test, control n=16, hypoxia n=17, p=0.1481). **(B)** 72h post-hypoxia (MW test, control n=16, hypoxia n=17, p=0.702).

A total number of 33 mice underwent the negative geotaxis test, 16 control and 17 hypoxia. 5 pups did not complete this test at 24h post-hypoxia (3 control, 2 hypoxia), and 8 did not at 72h post-hypoxia (3 control, 5 hypoxia). There was no significant difference in negative geotaxis times between the control and hypoxia groups at either 24h or 72h post-hypoxia (Figure 15.A-B). However, when applying the scoring system to account for non-participants,

there is a near-significant decrease (p=0.0994) in negative geotaxis response in hypoxia-exposed pups 72h post-hypoxia compared to healthy controls (Figure 15.C-D).

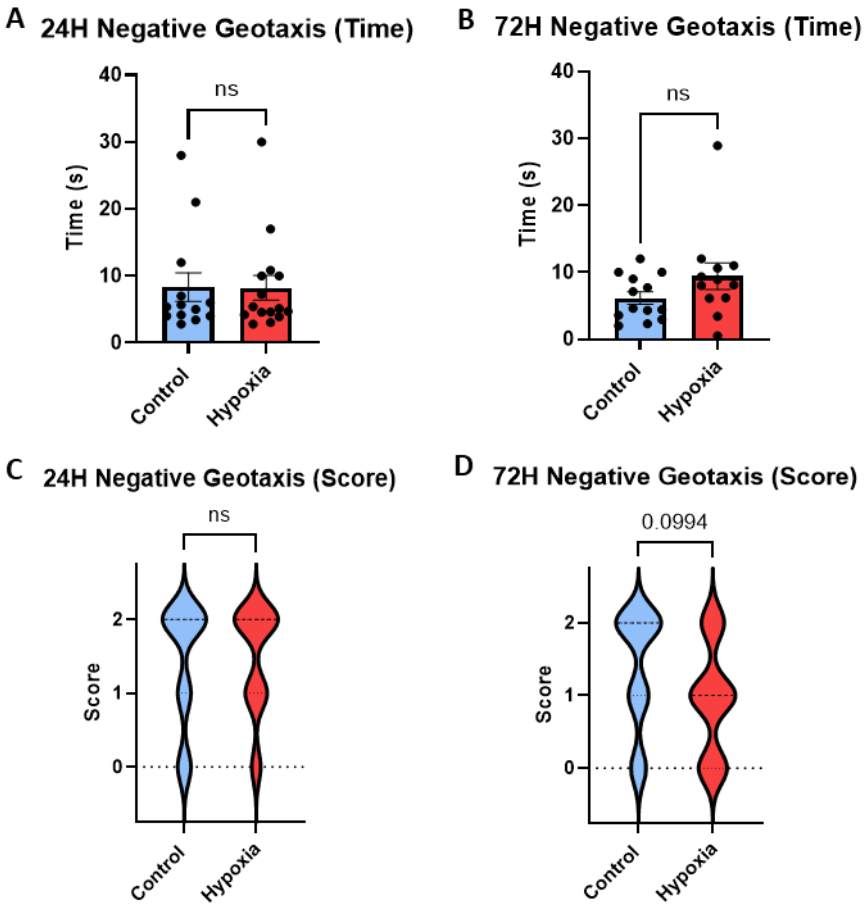

Figure 15: Negative geotaxis test results. Negative geotaxis times **(A)** 24h post-hypoxia (MW test, control n=13, hypoxia n=15, p=0.9008), **(B)** 72h post-hypoxia (MW test, control n=13, hypoxia n=12, p=0.1727). Negative geotaxis scores **(C)** 24h post-hypoxia (MW test, control n=16, hypoxia n=17, p=0.9999), **(D)** 72h post-hypoxia (MW test, control n=16, hypoxia n=17, p=0.0994).

A total number of 33 mice underwent the grip strength test, 16 control and 17 hypoxia. One control was excluded from the analysis at both 24h and 72h post-hypoxia due to non-participation. There was no significant difference in grip strength results between the control and hypoxia groups at either 24h or 72h post-hypoxia (Figure 16).

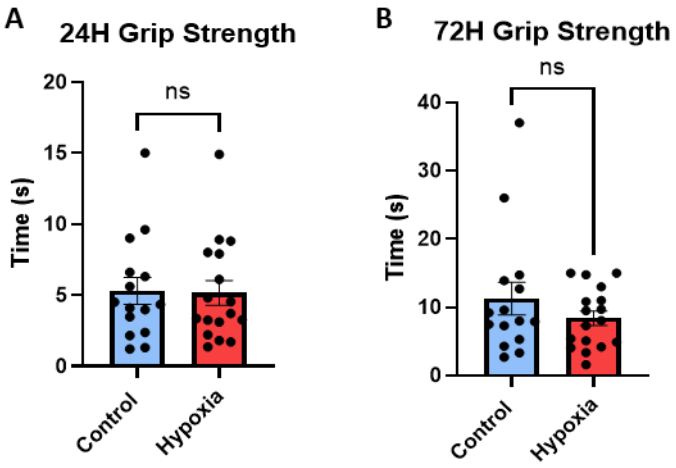

Figure 16: Grip strength test results. **(A)** 24h post-hypoxia (MW test, control n=15, hypoxia n=17, p=0.7944). **(B)** 72h post-hypoxia (MW test, control n=15, hypoxia n=17, p=0.7164).

A total number of 33 mice underwent the cliff aversion test, 16 control and 17 hypoxia. 2 litters were excluded from the analysis at both 24h (6 control, 6 hypoxia) and 72h (6 control, 7 hypoxia) post-hypoxia, due to a majority of non-participant controls from each litter. A further 6 pups did not participate at 24h post-hypoxia (2 control, 4 hypoxia), and 3 at 72h post-hypoxia (2 control, 1 hypoxia). There was no significant difference in litter-normalised cliff aversion times between the control and hypoxia groups at either 24h or 72h post-hypoxia (Figure 17.A-B). This was also no significant difference found when applying the scoring system to account for non-participants (Figure 17.C-D).

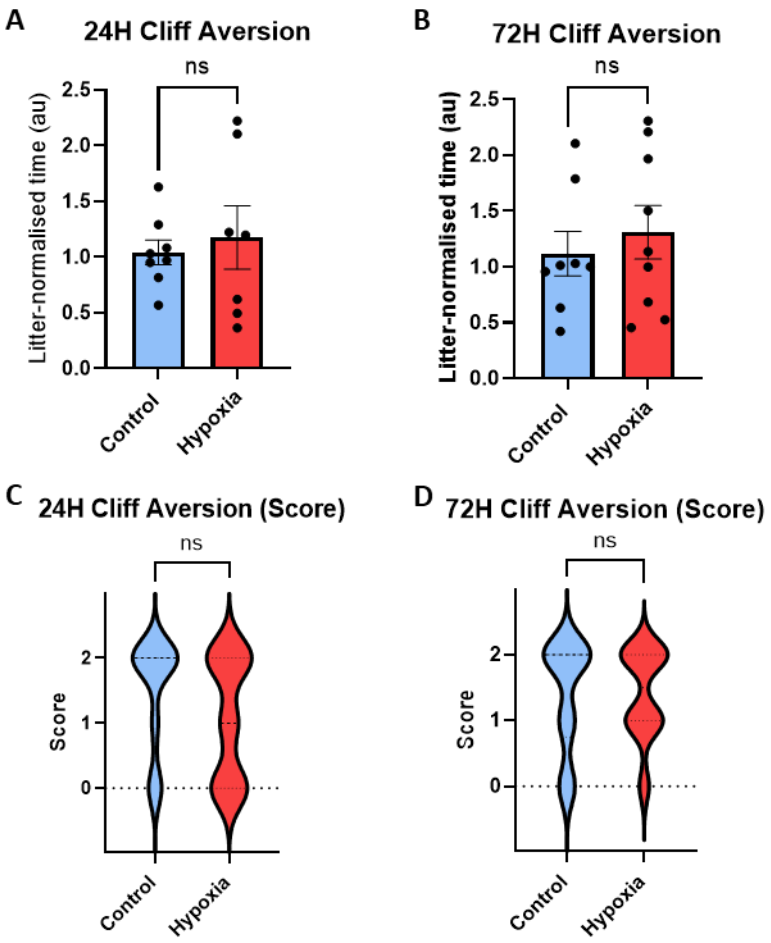

Figure 17: Cliff aversion test results. Litter-normalised times **(A)** 24h post-hypoxia (MW test, control n=8, hypoxia n=7, p=0.9551), **(B)** 72h post-hypoxia (MW test, control n=8, hypoxia n=9, p=0.6058). Cliff aversion scores **(C)** 24h post-hypoxia (MW test, control n=10, hypoxia n=11, p=0.3556), **(D)** 72h post-hypoxia (MW test, control n=10, hypoxia n=10, p=0.9999).

Adolescent behaviour

No significant difference in marble burying between hypoxia-exposed females and control females

A total of 17 mice underwent this test, 8 control (3 male, 5 female) and 9 hypoxia (4 male, 5 female). Analysis of marble burying results was divided by sex due to the possible influence of the oestrus cycle on burying activity (Schneider & Popik, 2007). This was the only behavioural test whose results were divided by sex as previous studies using the model found no sex differences in light-dark box, open field, or novel object location (Quinlan et al., 2019). One male in litter 2 (hypoxia mouse 7) displayed very aggressive behaviour, resulting in an increased anxiety response in the other males in the litter. The males in litter 3 displayed >10% weight loss and were euthanised before testing in line with the humane endpoints of this study. For this reason, only female results were included in the analysis. There was no

significant difference in marble burying observed between hypoxia-exposed females and control females (Figure 18.C).

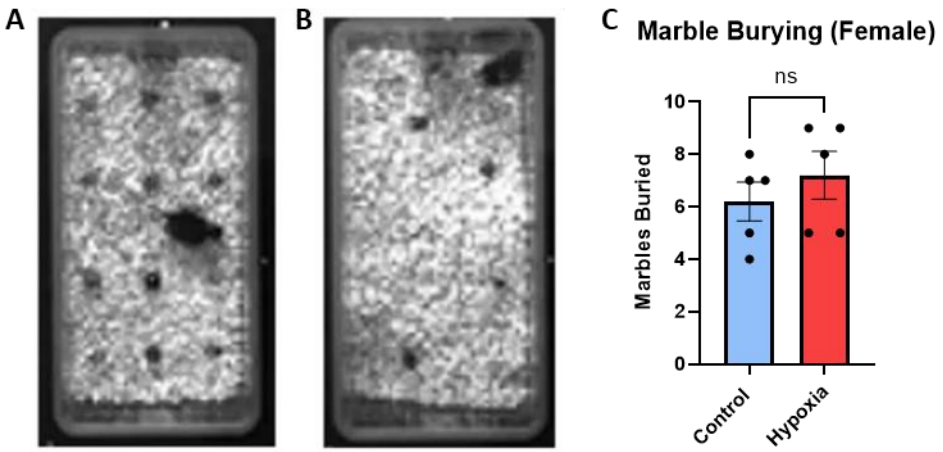

Figure 18: Marble burying results. Marble burying apparatus **(A)** before and **(B)** after the test. **(C)** Marbles buried by female mice (MW test, control n=5, hypoxia n=5, p=0.373).

Hypoxia-exposed mice differed from controls in the light-dark box test

A total number of 17 mice underwent this test, 8 control and 9 hypoxia. 3 videos did not start recording when the mouse was placed in the apparatus, so were excluded from the analysis of the latency to leave the light chamber for the first time. Similarly, 6 videos did not successfully track the movement of the mouse and were excluded from the subsequent analyses of time spent and distance travelled in the light chamber. Hypoxia-exposed mice spent significantly (p=0.0303) more time in the light box in comparison to controls (Figure 19.A). Near-significant increases in latency to leave the light chamber for the first time (p=0.0593) and distance travelled in the light chamber (p=0.0823) were also observed in hypoxic mice relative to controls (Figure 19.B-C).

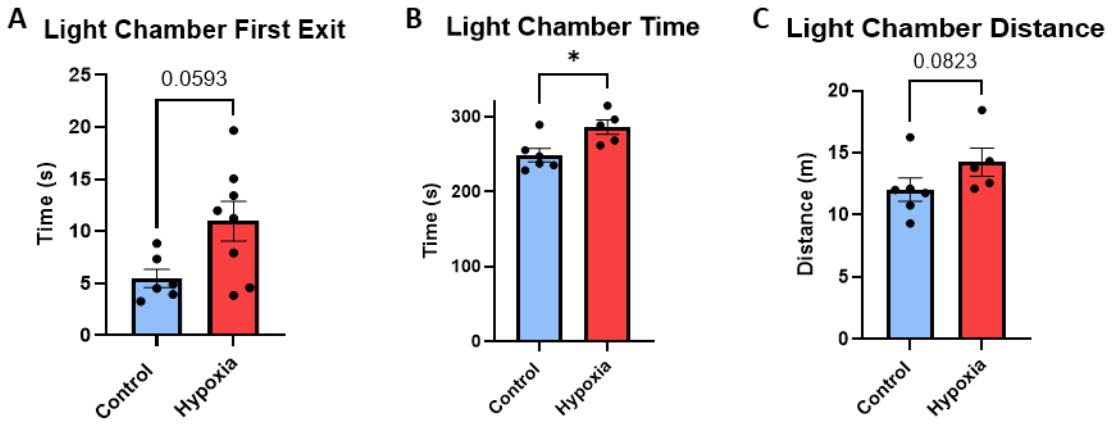

Figure 19: Light-dark box results. **(A)** Latency to first exit from the light chamber (MW test, control n=6, hypoxia n=8, p=0.0593). **(B)** Time spent in the light chamber (MW test, control n=6, hypoxia n=5, p=0.0303). **(C)** Distance travelled in the light chamber (MW test, control n=6, hypoxia n=5, p=0.0823).

Hypoxia-exposed mice differed from controls in the open field test

A total of 17 mice underwent this test, 8 control and 9 hypoxia. One control was excluded from all analyses due to a software failure to track the movement of the mouse. Over the 10 minutes, hypoxia-exposed mice travelled a significantly (p=0.0229) shorter distance than controls (Figure 20.A). They also spent significantly (p=0.0311) more time immobile, and when mobile, travelled at a significantly (p=0.0164) slower speed (Figure 20.B-C).

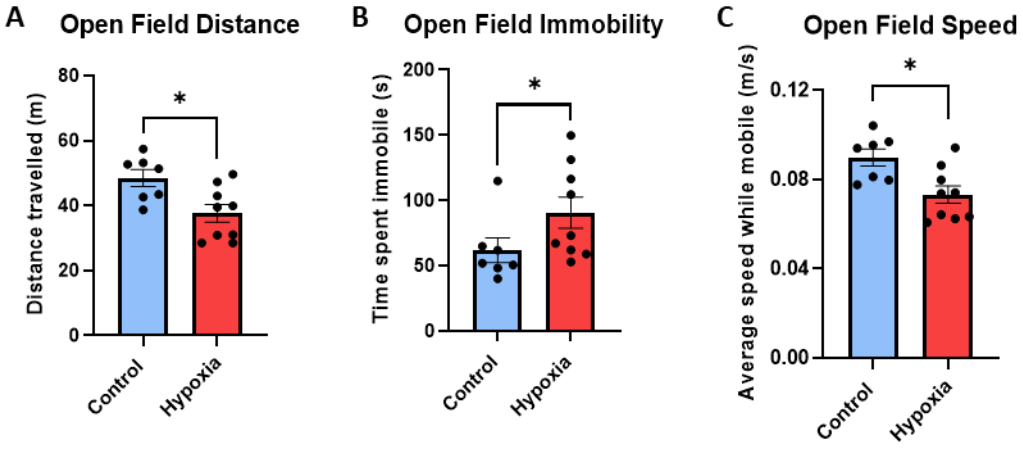

Figure 20: Open field test results. **(A)** Distance travelled in the open field (MW test, control n=7, hypoxia n=9, p=0.0229). **(B)** Time spent immobile in the open field (MW test, control n=7, hypoxia n=9, p=0.0311). **(C)** Average speed when mobile in the open field (MW test, control n=7, hypoxia n=9, p=0.0164).

Track plots and heatmaps of the open field test revealed that control mice were more peripheral in their movement compared to hypoxia-exposed mice (Figure 21.A-D). While there was no significant difference in the amount of time spent in the outer zone, hypoxic mice

spent significantly (p=0.0418) more time than controls in the inner zone of the enclosure (Figure 21.E-F).

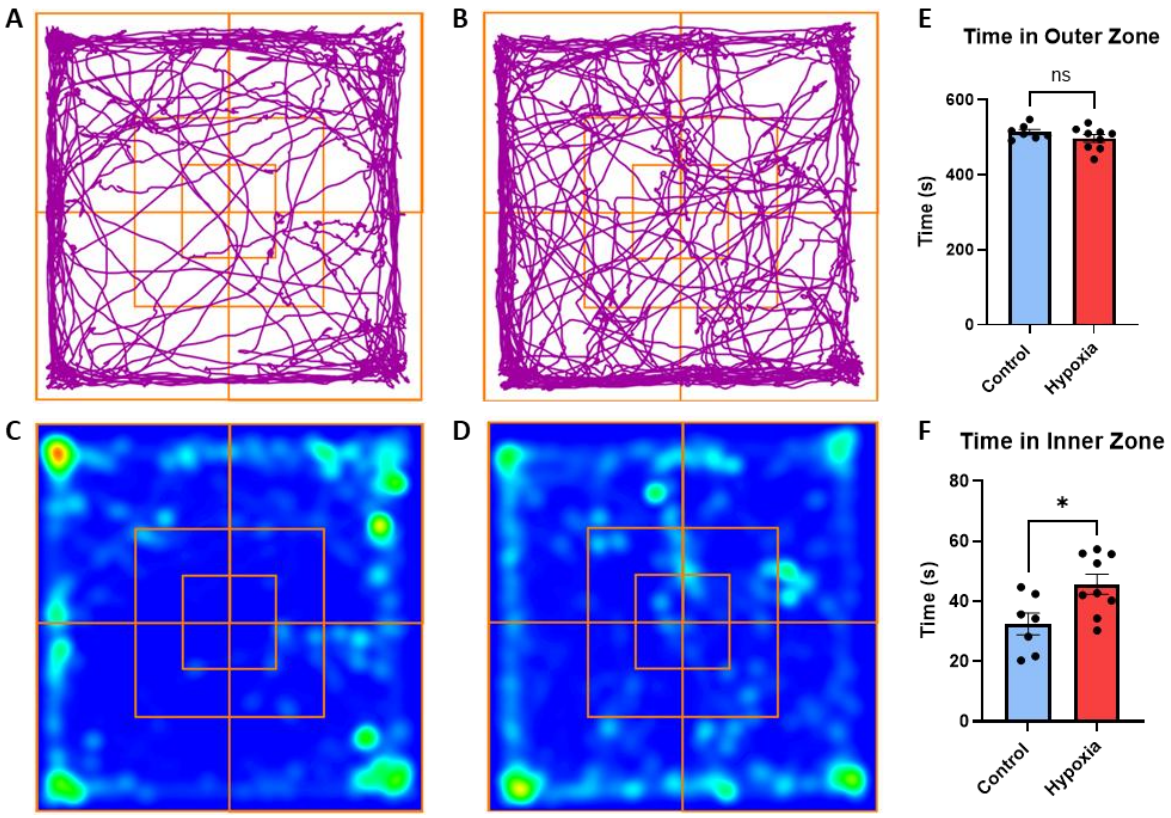

Figure 21: Open field track plots and heatmaps. Track plots of **(A)** control and **(B)** hypoxia-exposed adolescent mice. Heatmaps of **(C)** control and **(D)** hypoxia-exposed adolescent mice. Time spent in the **(E)** outer (MW test, control n=7, hypoxia n=9, p=0.4698) and **(F)** inner (MW test, control n=7, hypoxia n=9, p=0.0418) zones in the open field test.

Hypoxia-exposed mice spent less time in the novel object location compared to controls

A total of 17 mice underwent this test, 8 control and 9 hypoxia. Hypoxia-exposed mice spent significantly (p=0.036) less time with the object in the novel location than healthy controls (Figure 22.C). This was still true (p=0.0274) when adjusting for object preference shown in the familiarisation stage (Figure 22.D).

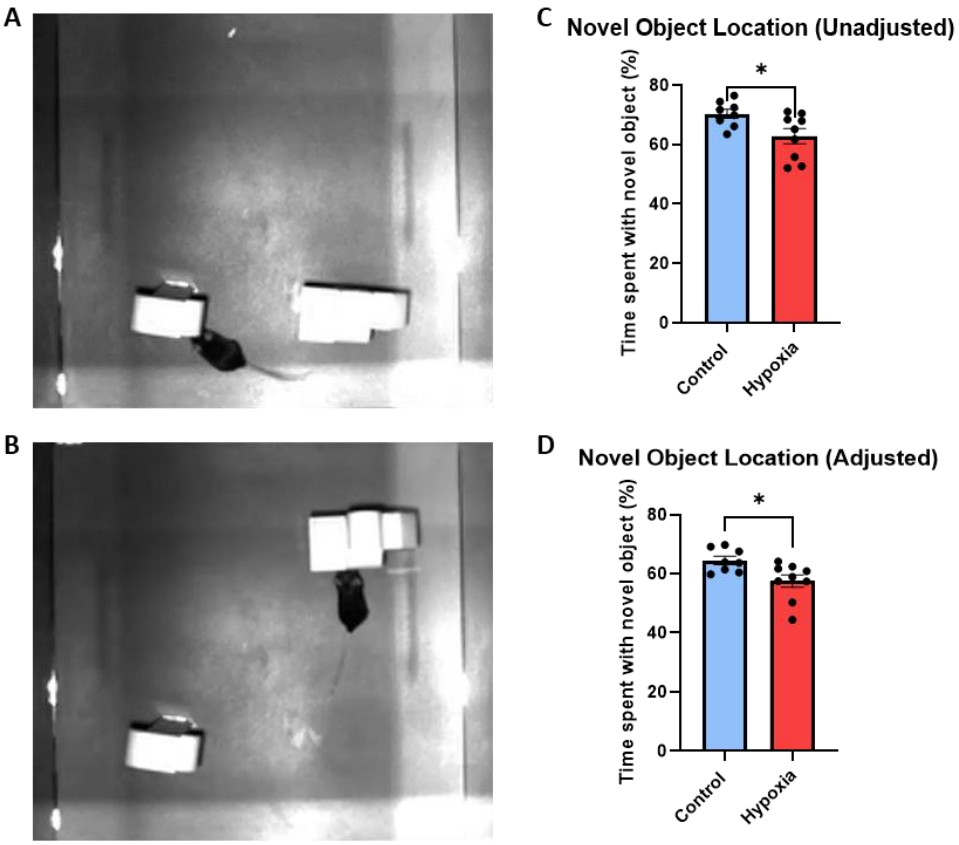

Figure 22: Novel object location test results. Apparatus setup for **(A)** familiarisation stage and **(B)** novel object location stage. Percentage of time spent with the object in the novel location **(C)** unadjusted for object preference (MW test, control n=8, hypoxia n=9, p=0.036) and **(D)** adjusted for object preference (MW test, control n=8, hypoxia n=9, p=0.0274).

MRI

No significant difference in hippocampal volume between hypoxia-exposed mice and controls

A total of 12 mice were scanned at P10, 6 control (3 male, 3 female) and 6 hypoxia (3 male, 3 female). A total of 11 mice were scanned at P42, 5 control (3 male, 2 female) and 6 hypoxia (2 male, 4 female). 6 P10 T1-weighted scans and one P42 T1-weighted scans were excluded from analysis due to a lack of contrast. All P10 T1-weighted data were thus excluded due to an insufficiently large sample size. There was no significant difference in hippocampal volume between hypoxia-exposed mice and controls at P10 in T2-weighted scans, or at P42 in either T1- or T2-weighted scans (Figure 23).

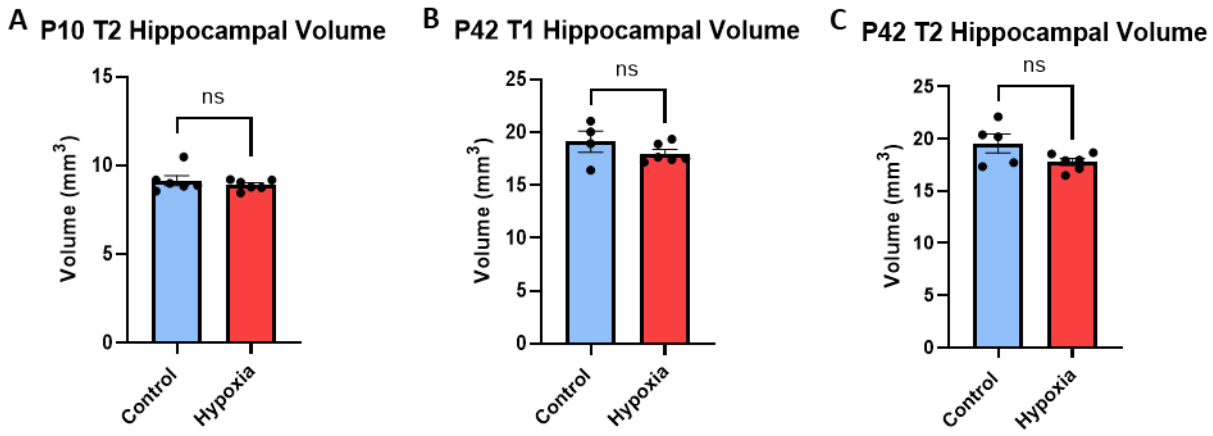

Figure 23: Hippocampal volume results. **(A)** P10 T2-weighted scans (MW test, control n=6, hypoxia n=6, p=0.6991). **(B)** P42 T1-weighted scans (MW test, control n=4, hypoxia n=6, p=0.3524). **(C)** P42 T2-weighted scans (MW test, control n=5, hypoxia n=6, p=0.2468).

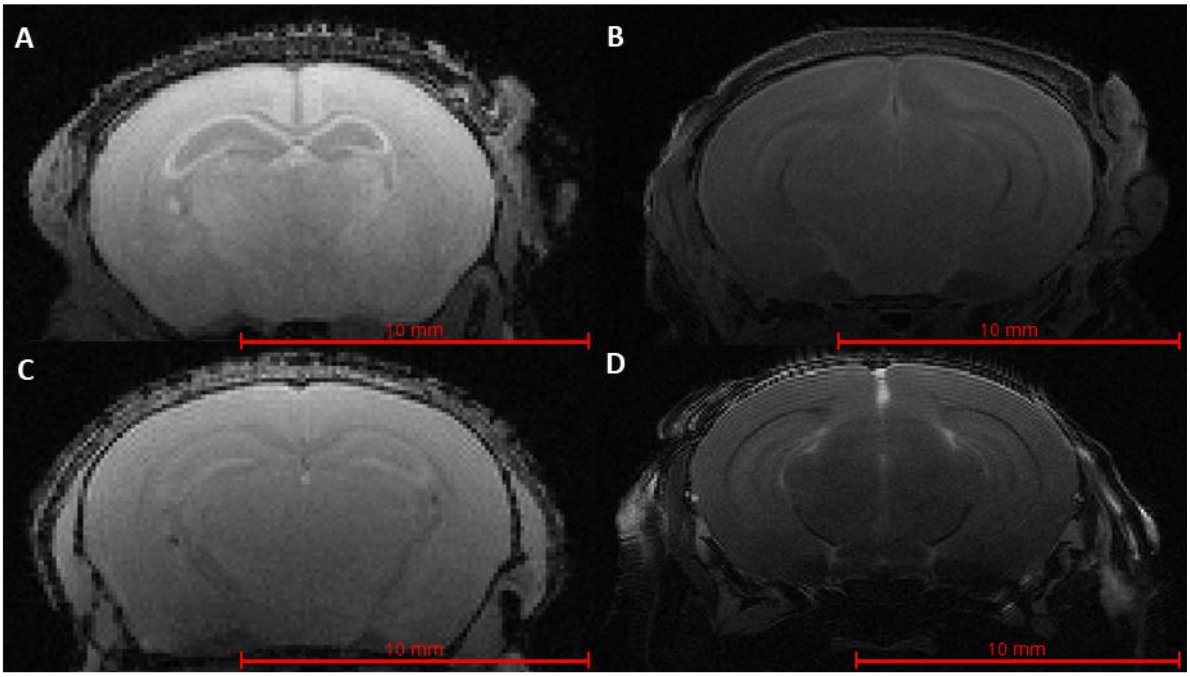

Figure 24: MRI scans. T1- and T2-weighted images of P10 and P42 mice. **(A)** T1-weighted P10 control. **(B)** T2-weighted P10 control. **(C)** T1-weighted P42 control. **(D)** T2-weighted P42 hypoxia.

Significantly more oedema exhibited in P42 hypoxia-exposed mice than in controls

No oedema was detected in any of the P10 T2-weighted images. However, in the P42 T2-weighted scans, significantly (p=0.0173) more cytotoxic oedema was detected in hypoxia-exposed mice than in controls (Figure 25.A). This cytotoxic oedema was present in the dorsal hippocampus alongside the dentate gyrus. All 6 mice that had undergone hypoxic induction had evidence of cytotoxic oedema.

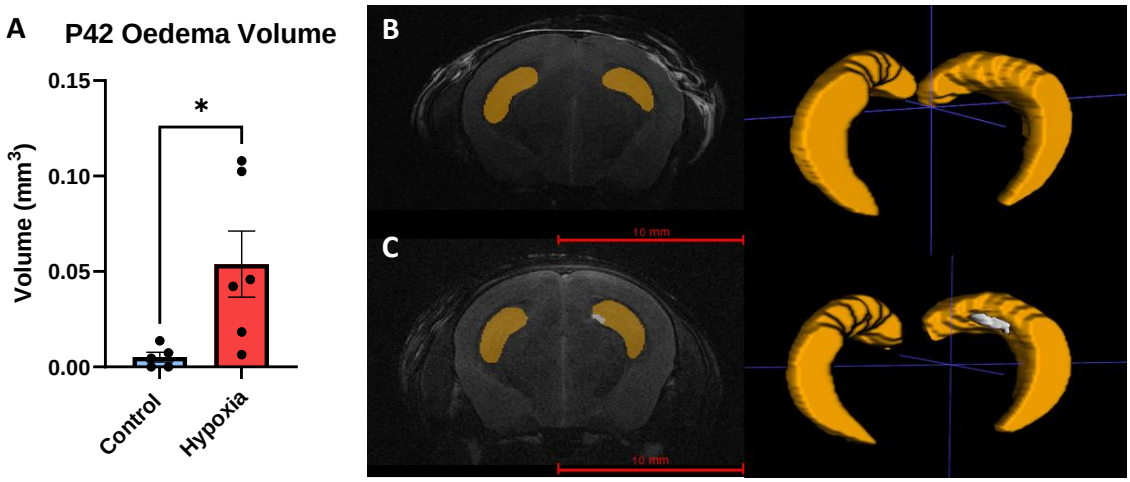

Figure 25: Oedema volume results. **(A)** Oedema volume in P42 hypoxic and control mice (MW test, control n=5, hypoxia n=6, p=0.0173). T2-weighted MRI segmentation results in **(B)** P42 control mouse and **(C)** P42 hypoxic mouse, with oedema (white) observed in the hippocampus (orange).

Significant correlation between oedema volume and adult behavioural tests

Having observed significant differences between control and hypoxia-exposed adolescent mice in both MRI and behavioural data, we decided to compare the two sets of results. Oedema volume was seen to correlate strongly with the performance of mice in adult behavioural tests. In the light-dark box test, more oedema correlated significantly with an increased latency to leave the light chamber for the first time (Figure 26.A). In the open field test, a greater volume of oedema correlated significantly with less distance travelled (Figure 26.B). In the novel object location test, more oedema correlated with less time spent with the object in the novel location (Figure 26.C).

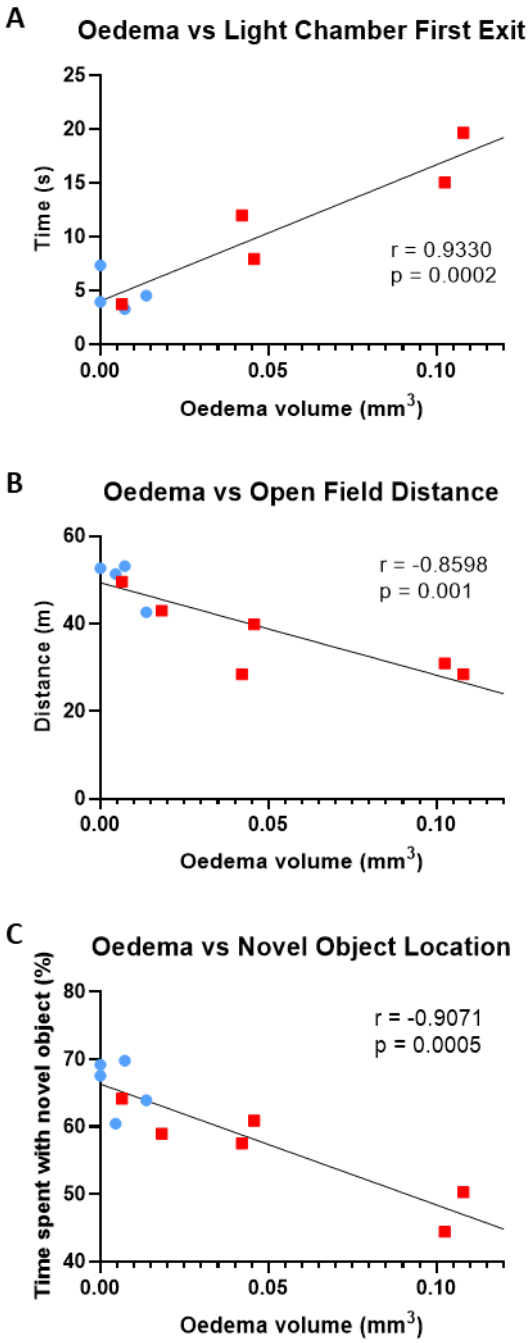

Figure 26: Correlation of oedema volume with behavioural tests. Pearson correlation of oedema volume with **(A)** latency to first light chamber exit in the light-dark box test (control n=4, hypoxia n=5, r=0.933, p=0.0002), **(B)** distance travelled in the open field test (control n=4, hypoxia n=6, r=-0.8598, p=0.001) and **(C)** time spent with the object in the novel location in the novel object location test (control n=5, hypoxia n=6, r=-0.9071, p=0.0005). Control mice are represented by blue circles, while hypoxia-exposed mice are represented by red squares.

Principal component analysis reveals distinct clusters for control and hypoxia behaviour

A total of 13 mice were included in this analysis, 5 control (2 male, 3 female) and 8 hypoxia (3 male, 5 female). 4 mice were excluded (3 control and 1 hypoxia) as they did not have complete data for the three behavioural tests considered (latency to first exit in the light-dark box test,

distance travelled in the open field test and time spent with the object in the novel location in the novel object location test). The first principal component accounted for 83.72% of the total explained variance (Figure 27); each of the three behavioural results contributed roughly equally to this principal component (loading values: light-dark box = 0.581, open field = -0.587, novel object location = -0.564). The control mice display a very tight clustering (mean Euclidean distance between points = 0.712), while the results of the hypoxia-exposed mice are widely dispersed (mean Euclidean distance between points = 3.094).

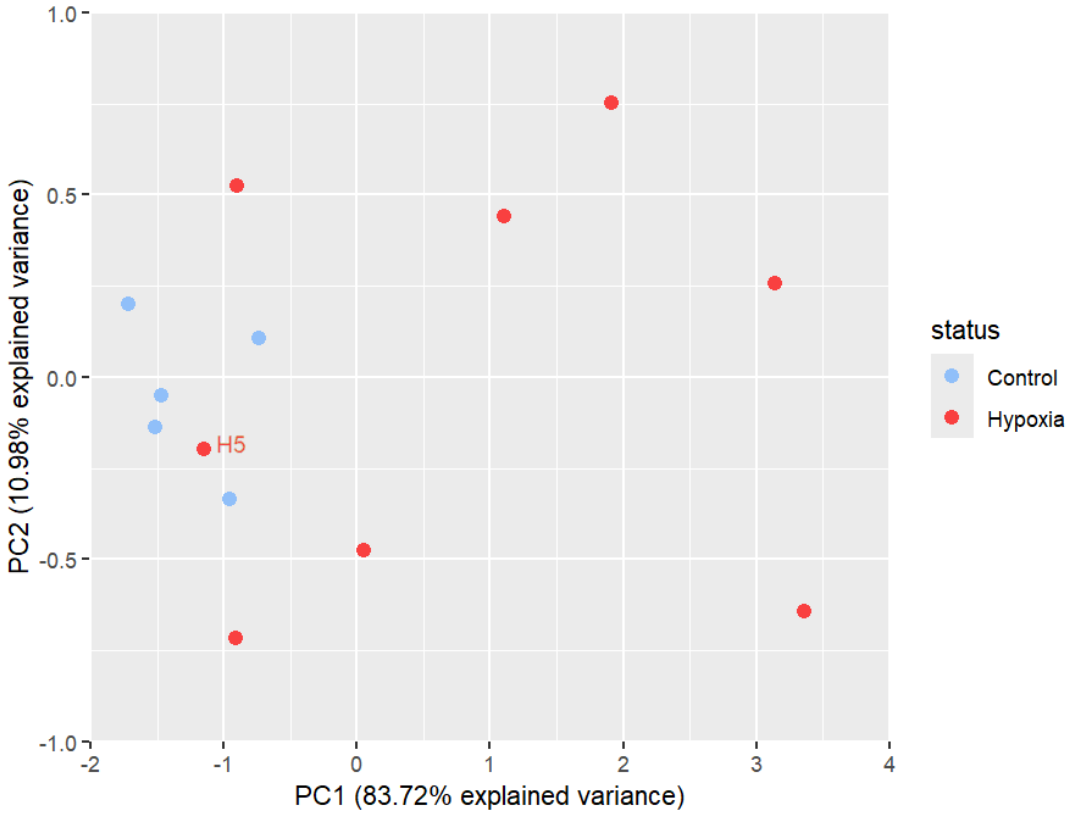

Figure 27: Principal component analysis of adolescent behaviour. Adolescent behaviour included consists of latency to first exit from the light chamber in the light-dark box test, distance travelled in the open field test, and percentage of time spent with the object in the novel location in the novel object location test (control n=5, hypoxia n=8). Hypoxia mouse 5 (H5) is labelled to highlight its position within the control cluster.

Discussion

Neonatal hypoxia is a severe condition with a complex pathophysiology and long-term neurodevelopmental consequences. This study demonstrates a potential link between hypoxia-induced cytotoxic oedema in the dorsal hippocampus and lasting cognitive and behavioural impairments. These findings highlight the need for early, accurate diagnosis to enable timely intervention and reduce long-term neurological complications.

Neonatal tests reveal delayed motor development in hypoxia-exposed pups

The ambulation test assesses the fluidity and symmetry of the walking movement and can be used to assess development. Hypoxia-exposed pups scored significantly lower than controls in the ambulation test 72h post-hypoxia (Figure 12.B), indicating a delayed transition from crawling to walking. Hypoxia-exposed mice also displayed significantly larger hindlimb foot angles than controls at the same time point (Figure 13.B), demonstrating deficits in motor development as a result of neonatal hypoxia. This supports the idea that substantial damage can occur in neonates when using a milder hypoxia model, as previously illustrated (Rodriguez-Alvarez et al., 2015).

While other results were not statistically significant, many indicated trends towards neurodevelopmental delays in hypoxia-exposed mice, with impairment more pronounced at 72h post-hypoxia compared to 24h, suggesting a widening gap over time. In particular, a near-significant deficit in negative geotaxis response is observed in hypoxic pups relative to controls at 72h post-hypoxia once non-participants are accounted for (Figure 15.D). This highlights the importance of a scoring system to include non-participants in analysis, as hypoxic injury may be contributing towards the non-participation.

Hypoxia-exposed mice exhibited an increase in anxiety-like behaviour

Mice who underwent hypoxia on P7 were tested between the fourth and sixth weeks of life over several behavioural aspects to assess the long-term outcomes (Eltokhi et al., 2020). The light-dark box test was used to investigate anxiety-related behaviour in mice, a test which is based on rodents' aversion to areas that are brightly illuminated (Bourin & Hascoët, 2003). As has been seen in a previous study using this same model (Rodriguez-Alvarez et al., 2015), hypoxia-exposed mice spent significantly more time in the light chamber than controls and travelled further in the light chamber compared to control mice (Figure 19). Additionally,

hypoxic mice spent significantly more time immobile than controls in the open field test (Figure 20.B). These results could be interpreted as an increase in anxiety-like behaviour. Further analysis with other anxiety tests, such as the elevated plus maze (Komada et al., 2008), may be required to corroborate these findings.

Hypoxia-exposed mice displayed impaired locomotor function

The open field test also revealed differences in locomotor function between hypoxic and control mice, with hypoxia-exposed mice travelling significantly less distance than controls, as well as a significantly lower average speed when mobile (Figure 20). This indicates that hypoxia exposure impacts neuromuscular development, as has been previously found (Rodriguez-Alvarez et al., 2015). However, this is inconsistent with previous research on the same model (Quinlan et al., 2018), which found that this model did not result in any locomotor dysfunction in adulthood.

Hippocampal function was impaired in hypoxia-exposed mice

The novel object location test was used to assess hippocampal-dependent object place recognition to evaluate long-term spatial memory in mice at five weeks post-hypoxia. The results found that hypoxic mice spent significantly less time with the novel object during the test period compared to controls, indicating some impairment in their long-term memory in this task (Figure 22). These results were largely consistent with those carried out using the same model previously, which also showed a deficit in hippocampus-dependent spatial memory function in hypoxic mice at 5 weeks post-hypoxia, and similar proportions of time spent with the novel object in control mice (Quinlan et al., 2018).

This pattern of cognitive impairment suggests a deficit in the dorsal hippocampus associated with spatial memory (Bannerman et al., 2014). This novel object location test is useful in categorising these hippocampal lesions compared to other novel object tests, such as the novel object recognition test (Denninger et al., 2018), which relies more heavily on multiple brain regions. However, hypoxia-induced vision changes such as retinal degeneration (Zaitoun et al., 2018) may have also contributed to impaired performance on this task. The textured novel object recognition test (Hayashi et al., 2024) could address concern this by using objects that are easier to detect through whisker sensitivity.

Cytotoxic oedema was a key marker of hypoxic injury

Oedema volume has been shown to be a key indicator of hypoxic brain injury severity (Biller et al., 2021). T2-weighted imaging in adult hypoxic mice showed a significantly greater dorsal hippocampal oedema volume than in control mice (Figure 25). This inflammation correlated with long-term behavioural impairments (Figure 26), suggesting that hypoxia-exposed mice experience more severe brain damage, specifically cytotoxic oedema in the dorsal hippocampus. In contrast, neonatal T2-weighted imaging did not visibly detect oedema (Figure 24.B). A hyperintense pyramidal layer surrounding the hippocampus seen in the T1-weighted image (Figure 24.A) may have obscured any oedema, preventing its identification in this study (Aggarwal et al., 2014).

Correlation analysis suggested oedema levels may be a stronger predictor of behavioural impairment outcomes than hypoxia status (Figure 26). This was evident in hypoxia mouse 5 (H5), which showed minimal oedema and displayed a behavioural phenotype more similar to that of control mice. PCA analysis supported this, with H5 positioned within the cluster of controls, while other hypoxia-exposed mice were more widely dispersed (Figure 27). This may reflect a variability in the manifestation of hypoxic injury between individuals, even those from the same litter. However, the small sample size (n=13) makes it difficult to draw robust conclusions from this result.

Physiological differences between neonatal & adult brain

Significant differences were observed between the MRI scans of the adult and neonatal brains, highlighting substantial structural and developmental changes in the brain from P10 to P42. The neonatal brain appeared darker in T2-weighted scans, particularly in the ventricles, and was more diffuse overall than the adult brain (Figure 24). This may result from higher water content and reduced compartmentalisation in the neonatal brain due to ongoing myelination (Olivieri et al., 2021). A hyperintense pyramidal layer visible in T1-weighted P10 scans was not as prevalent in P42 mice, which could be linked to the increased lipid content in cells during this developmental stage (Ferriero, 2004).

Cellular differences between neonatal and adult brains contribute to these distinct characteristics. Neonatal brains are more vulnerable to hypoxia due to higher unsaturated fatty acids concentrations, increased oxygen demand, and lower antioxidant capacity

(Ferriero, 2004). Preoligodendrocytes are highly sensitive to oxidative stress, often leading to selective white matter damage, whereas mature oligodendrocytes are more resistant due to their higher antioxidant capacity. Neonatal neutrophils have a reduced ability to migrate from blood vessels (Jiang et al., 1998), and their weaker lymphocyte response reflects immune system immaturity (Greco et al., 2020). These factors underscore the crucial role of the developmental stage in brain injury response.

Conclusion

This study provides insight into the anatomical brain changes associated with neonatal hypoxia, contributing to a better understanding of its neurological impact on behaviour and development in mouse models. This research highlights the profound and lasting consequences of neonatal hypoxia, particularly brain damage in the form of cytotoxic oedema. MRI analysis identified neuroanatomical alterations, including dorsal hippocampal damage persisting into adulthood. These structural changes were linked to cognitive and behavioural dysfunction, with global hypoxic injury delaying normal neonatal development and hippocampal damage correlating with long-term behavioural changes in adolescent mice.

Overall, these findings enhance our understanding of the pathological progression of hypoxic brain injury and help refine the classification of links between HIE-related injury and long-term neurological impairment. Importantly, these results also align with those outlined in human studies. Infants with HIE exhibit lower Denver scores, displaying delayed developmental milestones (Hallioglu et al., 2001). Children with a history of HIE are at risk of cognitive and behavioural difficulties in late childhood and adolescence (Lee & Glass, 2021). Observed similarities between hypoxia-induced neurodevelopmental impairment in mice and humans highlight the potential of this mouse model for translational studies regarding the pathophysiology and treatment of neonatal hypoxia.

Limitations

One limitation is that PFA fixation reduces MEMRI contrast over time (Sato et al., 2018). As a result, it is imperative to image the mice as soon as possible postmortem. Due to machine error, imaging of one litter was delayed by 48 hours, causing T1 contrast loss and subsequent exclusion of these images. Another limitation is that this study does not allow for the longitudinal comparison between MRI scans of the same mice at different time points. This would provide a more robust characterisation of what is happening throughout an individual's lifetime post-hypoxia induction. Additionally, hippocampal volumes were not normalised to total brain volume due to time constraints limiting MRI scans to the hippocampus, which prevented full brain segmentation in the T1-weighted scans. Future studies could address this for more reliable comparisons.

Future aims

This study can be expanded to assess structural and pathological damage in live mice post-hypoxia. The MRI protocol has been established as under 30 minutes, which is essential for minimizing maternal separation stress in developing an in vivo approach. T2-weighted MRI scans highlighted pathological changes post-hypoxia, but diffusion-weighted imaging (DWI) should be added for better differentiation between CSF and cytotoxic oedema. Cytotoxic oedema is characterised by ion accumulation within cells, leading to osmotic imbalance and intracellular fluid retention (Biller et al., 2021). DWI, which was not feasible for this project, detects cytotoxic oedema by decreased diffusion of water molecules (Schaefer et al., 1997). This would provide a deeper characterisation of post-hypoxia brain pathology and help determine differences in oedema between control and hypoxic brains.

Additionally, the use of automated segmentation techniques should be explored, in order to reduce human error and analysis time. One possible approach is using Markov random fields (Ali et al., 2005), in which each voxel is assigned to a class label conditional on its intensity and the labels of its neighbouring voxels. Such an approach could improve the precision of segmentations and enable a more in-depth classification system of anatomical and pathological features in the developing mouse brain.

References

Adams-Chapman. (2009). Insults to the developing brain and impact on neurodevelopmental outcome. *Journal of communication disorders, 42*(4), 256–62. https://doi.org/10.1016/j.jcomdis.2009.03.010

Adén, U., Dahlberg, V., Fredholm, B. B., Chen, Z., & Bjelke, B. (2002). MRI evaluation and functional assessment of brain injury after hypoxic ischemia in neonatal mice. *Stroke, 33*(5), 1405–1410. https://doi.org/10.1161/01.str.0000014608.78503.db

Aggarwal, M., Burnsed, J., Martin, L. J., Northington, F. J., & Zhang, J. (2014). Imaging neurodegeneration in the mouse hippocampus after neonatal hypoxia-ischemia using oscillating gradient diffusion MRI. *Magnetic resonance in medicine, 72*(3), 829–840. https://doi.org/10.1002/mrm.24956

Ali, A. A., Dale, A. M., Badea, A., & Johnson, G. A. (2005). Automated segmentation of neuroanatomical structures in multispectral MR microscopy of the mouse brain. *Neuroimage, 27*(2), 425–435. https://doi.org/10.1016/j.neuroimage.2005.04.017

Aslam, S., Strickland, T., & Molloy, E. J. (2019). Neonatal encephalopathy: need for recognition of multiple etiologies for optimal management. *Frontiers in pediatrics, 7*, 142. https://doi.org/10.3389/fped.2019.00142

Bannerman, D. M., Sprengel, R., Sanderson, D. J., McHugh, S. B., Rawlins, J. N., Monyer, H., & Seeburg, P. H. (2014). Hippocampal synaptic plasticity, spatial memory and anxiety. *Nature reviews neuroscience, 15*, 181–192. https://doi.org/10.1038/nrn3677

Biller, A., Badde, S., Heckel, A., Guericke, P., Bendszus, M., Nagel, A. M., . . . Schommer, K. (2021). Exposure to 16 h of normobaric hypoxia induces ionic edema in the healthy brain. *Nature communications, 12*(1), 5987. https://doi.org/10.1038/s41467-021-26116-y

Bourin, M., & Hascoët, M. (2003). The mouse light/dark box test. *European journal of pharmacology, 463*(1–3), 55–65. https://doi.org/10.1016/s0014-2999(03)01274-3

Brait, V. H., Wright, D. K., Nategh, M., Oman, A., Syeda, W. T., Ermine, C. M., . . . Brodtmann, A. (2021). Longitudinal hippocampal volumetric changes in mice following brain

infarction. *Scientific reports, 11*(1), 10269. https://doi.org/10.1038/s41598-021-88284-7

Chen, X., Chen, H., & Jiang, D. (2023). Maternal and fetal risk factors for neonatal hypoxic-ischemic encephalopathy: a retrospective study. *International journal of general medicine, 16*, 537–545. https://doi.org/10.2147/IJGM.S394202

de Brouwer, G., Fick, A., Harvey, B. H., & Wolmarans, D. W. (2019). A critical inquiry into marble-burying as a preclinical screening paradigm of relevance for anxiety and obsessive–compulsive disorder: Mapping the way forward. *Cognitive, affective, & behavioral neuroscience, 19*, 1–39. https://doi.org/10.3758/s13415-018-00653-4

Denninger, J. K., Smith, B. M., & Kirby, E. D. (2018). Novel object recognition and object location behavioral testing in mice on a budget. *Journal of visualized experiments : JoVE,* (141), 58593. https://doi.org/10.3791/58593

Doman, S. E., Girish, A., Nemeth, C. L., Drummond, G. T., Carr, P., Garcia, M. S., . . . Wilson, M. A. (2018). Early detection of hypothermic neuroprotection using T2-weighted magnetic resonance imaging in a mouse model of hypoxic ischemic encephalopathy. *Frontiers in neurology, 9*, 304. https://doi.org/10.3389/fneur.2018.00304

Douglas-Escobar, M., & Weiss, M. D. (2015). Hypoxic-ischemic encephalopathy: a review for the clinician. *JAMA pediatrics, 169*(4), 397–403. https://doi.org/10.1001/jamapediatrics.2014.3269

Ehlting, A., Zweyer, M., Maes, E., Schleehuber, Y., Doshi, H., Sabir, H., & Bernis, M. E. (2022). Impact of hypoxia-ischemia on neurogenesis and structural and functional outcomes. *Life (Basel, Switzerland), 12*(8), 1164. https://doi.org/10.3390/life12081164

Eltokhi, A., Kurpiers, B., & Pitzer, C. (2020). Behavioral tests assessing neuropsychiatric phenotypes in adolescent mice reveal strain- and sex-specific effects. *Scientific reports, 10*, 11263. https://doi.org/10.1038/s41598-020-67758-0

Feather-Schussler, D. N., & Ferguson, T. S. (2016). A battery of motor tests in a neonatal mouse model of cerebral palsy. *Journal of visualized experiments : JoVE,* (117), 53569. https://doi.org/10.3791/53569

Ferriero, D. M. (2004). Neonatal brain injury. *The New England journal of medicine, 351*(19), 1985–1995. https://doi.org/10.1056/NEJMra041996

Forcelli, P. A., Kozlowski, R., Snyder, C., Kondratyev, A., & Gale, K. (2012). Effects of neonatal antiepileptic drug exposure on cognitive, emotional, and motor function in adult rats. *The Journal of pharmacology and experimental therapeutics, 340*(3), 558–566. https://doi.org/10.1124/jpet.111.188862

Greco, P., Nencini, G., Piva, I., Scioscia, M., Volta, C. A., Spadaro, S., . . . Nappi, L. (2020). Pathophysiology of hypoxic-ischemic encephalopathy: a review of the past and a view on the future. *Acta neurologica Belgica, 120*(2), 277–288. https://doi.org/10.1007/s13760-020-01308-3

Hallioglu, O., Topaloglu, A. K., Zenciroglu, A., Duzovali, O., Yilgor, E., & Saribas, S. (2001). Denver developmental screening test II for early identification of the infants who will develop major neurological deficit as a sequalea of hypoxic-ischemic encephalopathy. *Pediatrics international: official journal of the Japan pediatric society, 43*(4), 400–404. https://doi.org/10.1046/j.1442-200x.2001.01418.x

Hayashi, Y., Alamir, N., Sun, G., Tamagnini, F., Hayashi, Y., Williams, C., & Zheng, Y. (2024). An effective textured novel object recognition test (tNORT) for repeated measure of whisker sensitivity of rodents. *Behavioural brain research, 472*, 115153. https://doi.org/10.1016/j.bbr.2024.115153

Jiang, N., Chopp, M., & Chahwala, S. (1998). Neutrophil inhibitory factor treatment of focal cerebral ischemia in the rat. *Brain research, 78*(1-2), 25–34. https://doi.org/10.1016/s0006-8993(97)01503-5

Kang, H. (2021). Sample size determination and power analysis using the G*Power software. *Journal of educational evaluation for health professions, 18*, 17. https://doi.org/10.3352/jeehp.2021.18.17

Komada, M., Takao, K., & Miyakawa, T. (2008). Elevated plus maze for mice. *Journal of visualized experiments : JoVE, 22*, 1088. https://doi.org/10.3791/1088

Lee, B. L., & Glass, H. C. (2021). Cognitive outcomes in late childhood and adolescence of neonatal hypoxic-ischemic encephalopathy. *Clinical and experimental pediatrics, 64*(12), 608–618. https://doi.org/10.3345/cep.2021.00164

Machie, M., Weeke, L., de Vries, L. S., Rollins, N., Brown, L., & Chalak, L. (2021). MRI score ability to detect abnormalities in mild hypoxic-ischemic encephalopathy. *Pediatric neurology, 116*, 32–38. https://doi.org/10.1016/j.pediatrneurol.2020.11.015

Oliveira, A. M., Hawk, J. D., Abel, T., & Havekes, R. (2010). Post-training reversible inactivation of the hippocampus enhances novel object recognition memory. *Learning & memory (Cold Spring Harbor, N.Y.), 17*(3), 155–160. https://doi.org/10.1101/lm.1625310

Olivieri, B., Rampakakis, E., Gilbert, G., Fezoua, A., & Wintermark, P. (2021). Myelination may be impaired in neonates following birth asphyxia. *Neuroimage clinical, 31*, 102678. https://doi.org/10.1016/j.nicl.2021.102678

Qiu, L. R., Fernandes, D. J., Szulc-Lerch, K. U., Dazai, J., Nieman, B. J., Turnbull, D. H., . . . Lerch, J. P. (2018). Mouse MRI shows brain areas relatively larger in males emerge before those larger in females. *Nature communications, 9*(1), 2615. https://doi.org/10.1038/s41467-018-04921-2

Quinlan, S. M., Rodriguez-Alvarez, N., Molloy, E. J., Madden, S. F., Boylan, G. B., Henshall, D. C., & Jimenez-Mateos, E. M. (2018). Complex spectrum of phenobarbital effects in a mouse model of neonatal hypoxia-induced seizures. *Scientific reports, 8*, 9986. https://doi.org/10.1038/s41598-018-28044-2

Quinlan, S., Merino-Serrais, P., Di Grande, A., Dussman, H., Prehn, J. H., Ní Chonghaile, T., . . . Jimenez-Mateos, E. M. (2019). The anti-inflammatory compound candesartan cilexetil improves neurological outcomes in a mouse model of neonatal hypoxia. *Frontiers in immunology, 10*, 1752. https://doi.org/10.3389/fimmu.2019.01752

Ristovska, S., Stomnaroska, O., & Danilovski, D. (2022). Hypoxic ischemic encephalopathy (HIE) in term and preterm infant. *Prilozi (Makedonska akademija na naukite i umetnostite. Oddelenie za medicinski nauki), 43*(1), 77–84. https://doi.org/10.2478/prilozi-2022-0013

Rodriguez-Alvarez, N., Jimenez-Mateos, E. M., Dunleavy, M., Waddington, J. L., Boylan, G. B., & Henshall, D. C. (2015). Effects of hypoxia-induced neonatal seizures on acute hippocampal injury and later-life seizure susceptibility and anxiety-related behavior in mice. *Neurobiology of disease, 83*, 100–114. https://doi.org/10.1016/j.nbd.2015.08.023

Sato, C., Sawada, K., Wright, D., Higashi, T., & Aoki, I. (2018). Isotropic 25-micron 3D neuroimaging using ex vivo microstructural manganese-enhanced MRI (MEMRI). *Frontiers in neural circuits, 12*, 110. https://doi.org/10.3389/fncir.2018.00110

Schaefer, P. W., Buonanno, F. S., Gonzalez, R. G., & Schwamm, L. H. (1997). Diffusion-weighted imaging discriminates between cytotoxic and vasogenic edema in a patient with eclampsia. *Stroke, 28*(5), 1082–1085. https://doi.org/10.1161/01.str.28.5.1082

Schindelin, J., Arganda-Carreras, I., Frise, E., Kaynig, V., Longair, M., Pietzsch, T., . . . Cardona, A. (2012). Fiji: an open-source platform for biological-image analysis. *Nature methods, 9*(7), 676–682. https://doi.org/10.1038/nmeth.2019

Schneider, T., & Popik, P. (2007). Attenuation of estrous cycle-dependent marble burying in female rats by acute treatment with progesterone and antidepressants. *Psychoneuroendocrinology, 32*(6), 651–659. https://doi.org/10.1016/j.psyneuen.2007.04.003

Shah, M. S. (2025). *Neonatal therapeutic hypothermia.* StatPearls Publishing.

Shah, P. S., & Perlman, M. (2009). Time courses of intrapartum asphyxia: neonatal characteristics and outcomes. *American journal of perinatology, 26*(1), 39–44. https://doi.org/10.1055/s-0028-1095185

Tetorou, K., Sisa, C., Iqbal, A., Dhillon, K., & Hristova, M. (2021). Current therapies for neonatal hypoxic-ischaemic and infection-sensitised hypoxic-ischaemic brain damage. *Frontiers in synaptic neuroscience, 13*, 709301. https://doi.org/10.3389/fnsyn.2021.709301

Volpe, J. J. (2001). Perinatal brain injury: from pathogenesis to neuroprotection. *Mental retardation and developmental disabilities research reviews, 7*(1), 56–64. https://doi.org/10.1002/1098-2779(200102)7:1<56::AID-MRDD1008>3.0.CO;2-A

Wickham, H. (2016). *ggplot2: Elegant Graphics for Data Analysis.* New York: Springer-Verlag. Retrieved from https://ggplot2.tidyverse.org

Wu, D., & Zhang, J. (2016). Progress in magnetic resonance imaging of the embryonic and neonatal mouse brain. *Frontiers in neuroanatomy, 10*, 18. https://doi.org/10.3389/fnana.2016.00018

Wu, J., Cai, Y., Wu, X., Ying, Y., Tai, Y., & He, M. (2021). Transcardiac perfusion of the mouse for brain tissue dissection and fixation. *Bio-protocol, 11*(5), 3988. https://doi.org/10.21769/BioProtoc.3988

Yıldız, E. P., Ekici, B., & Tatlı, B. (2017). Neonatal hypoxic ischemic encephalopathy: an update on disease pathogenesis and treatment. *Expert review of neurotherapeutics, 17*(5), 449–459. https://doi.org/10.1080/14737175.2017.1259567

Yushkevich, P. A., Piven, J., Hazlett, H. C., Smith, R. G., Ho, S., Gee, J. C., & Gerig, G. (2006). User-guided 3D active contour segmentation of anatomical structures: significantly improved efficiency and reliability. *Neuroimage, 31*(3), 1116–1128. https://doi.org/10.1016/j.neuroimage.2006.01.015

Zaitoun, I. S., Cikla, U., Zafer, D., Udho, E., Almomani, R., Suscha, A., . . . Sheibani, N. (2018). Attenuation of retinal vascular development in neonatal mice subjected to hypoxic-ischemic encephalopathy. *Scientific reports, 8*, 9166. https://doi.org/10.1038/s41598-018-27525-8

Zanier, E. R., Pischiutta, F., Villa, P., Paladini, A., Montinaro, M., Micotti, E., . . . De Simoni, M. G. (2013). Six-month ischemic mice show sensorimotor and cognitive deficits associated with brain atrophy and axonal disorganization. *CNS neuroscience & therapeutics, 19*(9), 695–704. https://doi.org/10.1111/cns.12128

Zhou, Z., Bai, R., Munasinghe, J., Shen, Z., Nie, L., & Chen, X. (2017). T1–T2 dual-modal magnetic resonance imaging: from molecular basis to contrast agents. *ACS Nano, 11*(6), 5227–5332. https://doi.org/10.1021/acsnano.7b03075